

# Lock-In Amplifier Architectures for Sub-ppm Resolution Measurements

Giacomo Gervasoni, Marco Carminati and Giorgio Ferrari

**Abstract** Ideally, lock-in amplifiers (LIAs) would be able to measure a minimum signal variation limited by the noise of the front-end amplifier and the filtering bandwidth. On the contrary, a detailed characterization of digital LIAs shows an unforeseen  $1/f$  noise at the instruments demodulated output, proportional to the total signal amplitude. The signal-proportionality and  $1/f$  nature of the measured noise pose a fundamental limit to the LIAs achievable resolution. This limit has been found to be dependent from the instrument maximum operating frequency, from few ppm for LIAs operating up to few hundreds of kHz, to few tens of ppm for LIAs operating up to few MHz or tens of MHz. The additional noise is due to slow gain fluctuations that the signal experiences from the generation stage to the acquisition one. To compensate them, a switched ratiometric technique based on two ADCs alternately acquiring the signal coming from the device under test and the stimulus signal has been conceived. The idea is that both signals should experience the same gain fluctuations, which can be successively removed by means of a division on the outputs of the synchronous demodulation. An FPGA-based LIA working up to 10 MHz and implementing the technique has been realized and results demonstrate a resolution improvement of more than an order of magnitude compared to standard implementations working up to similar frequencies (from tens of ppm down to sub-ppm values).

## 1 Introduction

Lock-in amplifiers (LIAs) are extensively used for synchronous (phase-sensitive) AC signals detection and measurement in a wide range of scientific fields [1]. Two main reasons justify such a widespread application of LIAs [2]. First, the idea of translating signals in frequency domain (signal modulation), instead of performing DC measurements, arises from the ubiquitous presence of static errors and  $1/f$  noise,

---

G. Gervasoni · M. Carminati · G. Ferrari (✉)  
Politecnico di Milano, Dipartimento di Elettronica, Informazione e Bioingegneria,  
Piazza Leonardo da Vinci, 32, 20133 Milano, Italy  
e-mail: giorgio.ferrari@polimi.it

© Springer International Publishing AG 2017  
B. George et al. (eds.), *Advanced Interfacing Techniques for Sensors*,  
Smart Sensors, Measurement and Instrumentation 25,  
DOI 10.1007/978-3-319-55369-6\_6

given by electronic circuits, devices, sensors or other elements taking part into experiments. The frequency of the measurement is easily selectable using a LIA architecture allowing an operation in the frequency range where the signal-to-noise ratio is maximum. Secondly, the physics of the experiment itself can impose an AC measurement, as in the case of sensors based on impedance measurements, capacitance measurements or resonant phenomena. In both cases, a LIA extracts the amplitude and phase of the AC signal from the background noise and spurious signals with an excellent frequency selectivity, thus combining the advantages of an AC measurement with an optimal signal-to-noise ratio. State-of-the-art lock-in instruments are able to measure voltage signals down to a few nV in a wide range of operating conditions.

For some sensors it is necessary to detect very small variations of an electrical parameter (such as current, resistance or capacitance) with respect to a relatively large baseline value [3–7]. As an example, sensors for counting the number of cells in a liquid [8, 9] or the number of airborne particulate matter [10] can be obtained with an impedance measurement. The fluid under investigation is forced to flow between two electrodes or over them. When no particles are in the volume sensed by the electrodes, the impedance is related to the electrical properties of the fluid and to the geometry of the electrodes. When a particle passes in the sensed volume, the impedance of the sensor changes of a quantity related to the volume of the particle and to its electrical properties. Thus, by monitoring the impedance variations in the time, it is possible to count the number of particles flowing in the fluid. The capability of counting particles with a small (micrometric) size imposes a sensor interface able to sense the correspondingly tiny impedance change superposed to the impedance of the fluid, i.e. a high resolution measurement is required.

Here we discuss the limitations to the best resolution achievable with digital LIAs and how to overcome them. The main noise sources playing a role in measurements with ppm resolution are identified in Sect. 3 and two methods are described to reduce their effects. The first method, described in Sect. 4, is the well-known differential approach where the signal from the sensor is measured with respect to a reference device. By applying to the sensor and to the reference the same stimulus signal and by choosing a reference as similar as possible to the sensor, the baseline signal is effectively reduced, thus relaxing the specification of the LIA in terms of resolution. When a reference path, matching the sensor parameters for all the experimental conditions, is unpractical, it is necessary to design a LIA specifically conceived for high resolution measurements. The second part of the chapter (Sects. 5, 6 and 7) discusses an enhanced lock-in amplifier able to reach sub-ppm resolution in a wide range of operating frequencies without requiring a reference device.

## 2 Lock-In Amplifier Working Principle

Figure 1 describes a simplified schematic of a lock-in amplifier. A sinusoidal stimulus  $A \cos(2\pi f_0 t)$  is generated and applied to a generic Device Under Test (DUT)

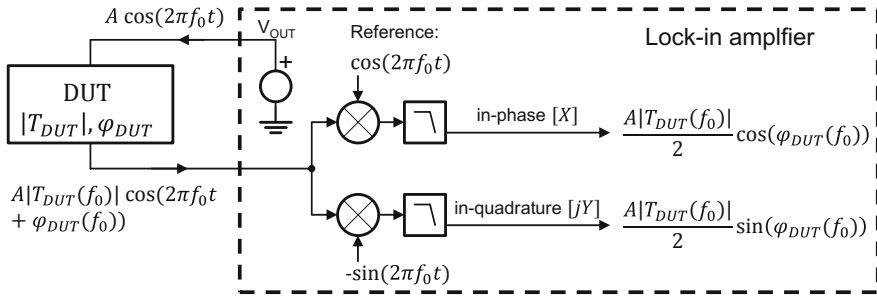


Fig. 1 Simplified scheme of a Lock-In Amplifier

that includes all the elements between the output of the LIA and its input. The sinusoidal stimulus is modified in amplitude and in phase by the transfer function  $T_{DUT}(f)$  at the operating frequency  $f_0$ . The lock-in amplifier acquires the signal coming from the DUT and multiplies it in parallel by two sinusoidal signals, synchronous with the stimulus signal:  $\cos(2\pi f_0 t)$  to obtain the in-phase component and  $-\sin(2\pi f_0 t)$  to obtain the in-quadrature one. Both multiplications provide two terms, the first one in DC, while the second one at the double of the working frequency ( $2f_0$ ). The second term is cancelled out through low-pass filtering, while the first terms<sup>1</sup>  $X = \frac{1}{2}A|T_{DUT}| \cos(\varphi_{DUT})$  and  $Y = \frac{1}{2}A|T_{DUT}| \sin(\varphi_{DUT})$  are respectively proportional to the in-phase and quadrature components of the input signal. From these two outputs, also the signal modulus and phase can be easily obtained:  $R = 2\sqrt{X^2 + Y^2} = A|T_{DUT}|$  and  $\varphi_{DUT} = \arctan(\frac{Y}{X})$ .

For high sensitivity measurements, it is useful to calculate the Signal-to-Noise Ratio ( $SNR_{OUT}$ ) at the output of the lock-in amplifier. First, from the previous calculations it is possible to define the LIA signal power gain, defined as the ratio between the power of the output DC signal  $P(V_{out,DC})$  and the power of the input sinusoidal signal  $P(V_{in,AC})$ , obtaining:

$$G_{Sign\ Power,X} = \frac{P(V_{out,DC,X})}{P(V_{in,AC})} = \frac{\left(\frac{A|T_{DUT}| \cos(\varphi_{DUT})}{2}\right)^2}{\frac{(A|T_{DUT}|)^2}{2}} = \frac{\cos^2(\varphi_{DUT})}{2} \quad (1)$$

$$G_{Sign\ Power,Y} = \frac{P(V_{out,DC,Y})}{P(V_{in,AC})} = \frac{\left(\frac{A|T_{DUT}| \sin(\varphi_{DUT})}{2}\right)^2}{\frac{(A|T_{DUT}|)^2}{2}} = \frac{\sin^2(\varphi_{DUT})}{2} \quad (2)$$

<sup>1</sup>Here and in the successive calculations  $|T_{DUT}|$  and  $\varphi_{DUT}$  are the magnitude and the phase of the transfer function  $T_{DUT}(f)$  at the working frequency  $f_0$ .

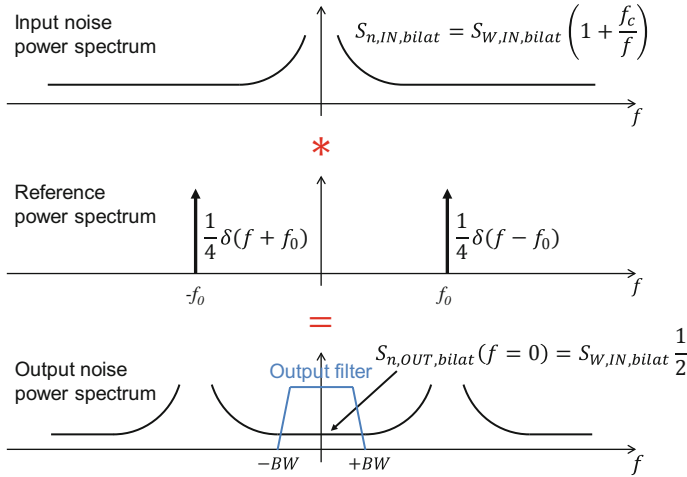


**Fig. 2** Frequency shifting and power scaling of the input noise in lock-in amplifiers in the case of  $f_0 \gg f_c$

In order to compute the LIA output  $SNR_{OUT}$ , it is also necessary to calculate how the noise at the input of the LIA is transferred to the output. To do it, an analysis in the frequency domain using the power spectral density of the noise is preferable to a time domain analysis. Looking at the in-phase component extraction chain, the multiplication by the sinusoidal signal  $\cos(2\pi f_0 t)$  corresponds, in the frequency domain, to a convolution operation that scales and shifts the power spectral density of the noise at the input around  $\pm f_0$  as shown in Fig. 2. The noise power density gain is defined as the ratio between the output noise at  $f = 0$  and the input noise at the LIA operating frequency  $f_0$ :

$$G_{Noise \text{ Power Density}} = \frac{S_{n,OUT,bilat}(0)}{S_{n,IN,bilat}(f_0)} = \frac{S_{n,IN,bilat}(f_0) \frac{1}{2}}{S_{n,IN,bilat}(f_0)} = \frac{1}{2} \quad (3)$$

where  $S_{n,IN,bilat}$  and  $S_{n,OUT,bilat}$  are the bilateral power spectral density of the input and output noise, respectively. The same result is obtained for the in-quadrature chain.

The power of the noise at the output is obtained by integrating the output power spectral density in the bandwidth of the low-pass filter. Usually the bandwidth is much smaller of the operating frequency  $f_0$  for an effective reduction of the noise and of the spurious harmonics at the output of the demodulator. In this condition the output noise spectral density is commonly assumed white in the bandwidth of the filter irrespective of the frequency dependence of the input spectral density [1, 11, 12]. Consequently, the noise integration in the bandwidth of the low-pass filter is obtained with a multiplication of the spectral density by the equivalent noise bandwidth of the filter. Then, by considering for simplicity the case of the input signal in

the in-phase output<sup>2</sup> ( $\varphi_{DUT} = 0$ ), the LIA  $SNR_{OUT}$  is:

$$\begin{aligned} SNR_{OUT} &= \frac{P_{OUT,Sign}}{P_{OUT,Noise}} = \frac{P_{IN,Sign} G_{Sign} Power X}{S_{n,IN,bilat}(f_0) G_{Noise} Power Density 2BW} \\ &= \frac{P_{IN,Sign} \frac{1}{2}}{S_{n,IN,bilat}(f_0) \frac{1}{2} 2BW} = \frac{P_{IN,Sign}}{S_{n,IN,mono}(f_0) BW} \end{aligned} \quad (4)$$

where  $BW$  is the equivalent noise bandwidth of the low-pass filter and  $S_{n,IN,bilat} = S_{n,IN,mono}/2$  by definition. Equation 4 confirms the LIA efficiency in extracting the information from a sinusoidal signal:  $SNR_{OUT}$  is simply given by the ratio between the rms value of the input sinusoidal signal and the input noise density at  $f_0$  integrated in the noise bandwidth  $BW$  without a degradation of the  $SNR$  at the input of the LIA. This excellent result on the  $SNR$  of the measurement is obtained with additional advantages compared to a direct AC measurement of the signal: (i) simplicity in the selection of the operating frequency  $f_0$ ; (ii) a small bandwidth is feasible independently of  $f_0$  without the implementation of a tuned band-pass filter as required for a standard AC measurement; (iii) both the in-phase and quadrature components are available as DC values at the output of the instrument.

## 2.1 Digital Lock-In Amplifiers

Early LIAs were designed with analog electronics, while digital designs of the low-pass filters emerged in the 1980s. By the early 1990s even the analog demodulators were replaced by high-resolution ADCs and Digital Signal Processors (DSPs). The capabilities of modern DSP-based LIAs in stability, dynamic reserve, and flexibility were revolutionary, making them a mainstay for researchers and engineers. Nowadays, powerful Field Programmable Gate Arrays (FPGAs) are widely used to perform the digital processing required by fast (up to 600 MHz, UHFLI by Zurich Instruments) digital LIAs, whose basic functional scheme is represented in Fig. 3. The FPGA generates the in-phase and in-quadrature reference signals in the digital domain using a Direct Digital Synthesizer (DDS). An output stage based on a digital-to-analog converter (DAC) and a programmable gain amplifier (PGA) generates the output analog signal  $V_{OUT}$ . The amplitude of the input signal of the LIA is amplified by a second PGA and low-pass filtered by a wide bandwidth anti-aliasing filter. The digital samples obtained by the analog-to-digital converter (ADC) are demodulated and filtered by the FPGA.

---

<sup>2</sup>This condition can be easily obtained in a digital LIA by adjusting the phase of the internal reference by a factor  $\varphi_{DUT}(f_0)$ .

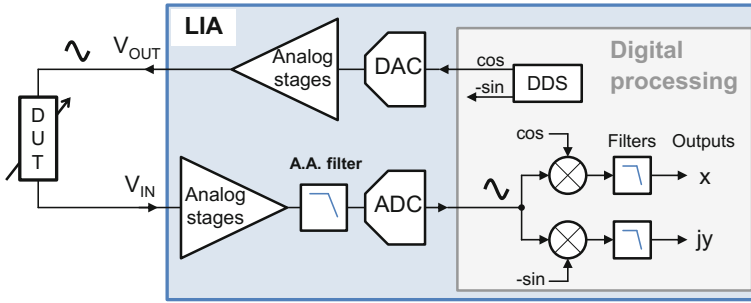


**Fig. 3** Basic scheme of a digital lock-in amplifier (LIA) connected to a generic Device Under Test (DUT)

### 3 Resolution Limit of Digital Lock-In Amplifiers

As shown in Sect. 2, the minimum detectable signal of a lock-in amplifier depends on its input equivalent noise at the working frequency  $f_0$  and the chosen filtering bandwidth  $BW$ . State-of-the-art instruments show an input equivalent noise as low as few  $\text{nV}/\sqrt{\text{Hz}}$  when used with an input range of few mV.

Ideally, the minimum detectable signal *variation* of a LIA is independent of the signal amplitude given a fixed input range. On the contrary, experimental evidence shows that digital lock-in amplifiers have an unforeseen  $1/f$  output noise proportional to the measured signal [13]. Consequently, when this contribution becomes dominant, the minimum detectable signal variation becomes proportionally dependent to the total signal itself and orders of magnitude greater than the expected minimum detectable signal. Moreover, being the additional noise with a  $1/f$  spectrum, it can not be effectively low-pass filtered, posing a fundamental limit to the lock-in amplifier relative resolution, defined as the ratio between the minimum detectable signal variation and the total signal itself and expressed in ppm. In the following, the relative resolution will be simply called resolution in absence of ambiguity.

Table 1 shows the resolution experimentally measured with different LIAs when the stimulus signal is directly connected to the input of the instrument. The bandwidth was set to 1 Hz and the relative resolution are calculated on a time duration of 100 s.

Results show that the instruments resolution limit can not be improved by increasing the stimulus amplitude or by changing the operating frequency. The LIAs resolution are related to the instrument maximum operating frequency, from few ppm for LIAs operating up to few hundreds of kHz, to few tens of ppm for instruments operating up to few MHz or tens of MHz. The distinctive results obtained with the successively presented Enhanced-LIA (ELIA) are highlighted in red.

**Table 1** Experimental comparison of LIA performances. Test conditions are: stimulus signal directly connected to the LIA input, bandwidth of 1 Hz and measurement time of 100 s. The custom LIAs are described in [14, 15]

Model	Maximum frequency [MHz]	Signal amplitude [V]	Measurement frequency [MHz]	Relative resolution [ppm]
Custom LIA [14]	0.1	0.1, 0.3, 1	0.01, 0.05	1
SR830 (Stanford Research Systems)	0.1	0.1, 0.3, 1	0.01, 0.05	12
MCL1-540 (SynkTek)	0.5	1.4	0.1	1.3
SR865 (Stanford Research Systems)	2	0.3	0.5	45
Custom LIA [15]	10	0.03, 0.1, 0.3, 1	0.1, 1	9
HF2LI (Zurich Instruments)	50	0.03, 0.1, 0.3, 1	0.1, 1, 10	39
Enhanced-LIA (Section 5)	10	0.1, 0.3, 1	0.0001-6 6-10	0.6-1 1-3.5

### 3.1 Lock-In Amplifiers Noise Experimental Characterization

In order to deeply understand the results reported in Table 1, the noise of the state-of-the-art lock-in amplifier HF2LI by Zurich Instruments has been characterized and analyzed. A 1 MHz sinusoidal stimulus ranging from 0 to 1 V has been generated at the instrument output and directly connected to its input (Fig. 4a, top). In all measurements the input and output range have been set at 1.1 V and 1 V respectively. The signal, after synchronous demodulation, is filtered (80 kHz bandwidth) and acquired. The FFT is performed and the results are shown in Fig. 4a.

In the absence of signal (stimulus voltage  $V_{OUT}$  set to 0 V) the demodulated signal shows a white noise equal to the noise of the analog front-end at 1 MHz, as expected. However, as the sinusoidal signal amplitude increases, additional  $1/f$  noise proportional to the signal amplitude appears. The same behavior has been observed with all tested LIAs.

As already mentioned, this signal-proportional  $1/f$  noise produces two drawbacks: (i) due to the  $1/f$  spectral distribution, narrowing the filter bandwidth is no more effective in order to reduce the output noise of the instrument; (ii) increasing the signal amplitude does not improve the measurement resolution due to the concomitant noise increase. As a consequence, when dominated by this  $1/f$  noise, the LIA reaches its ultimate resolution limit.

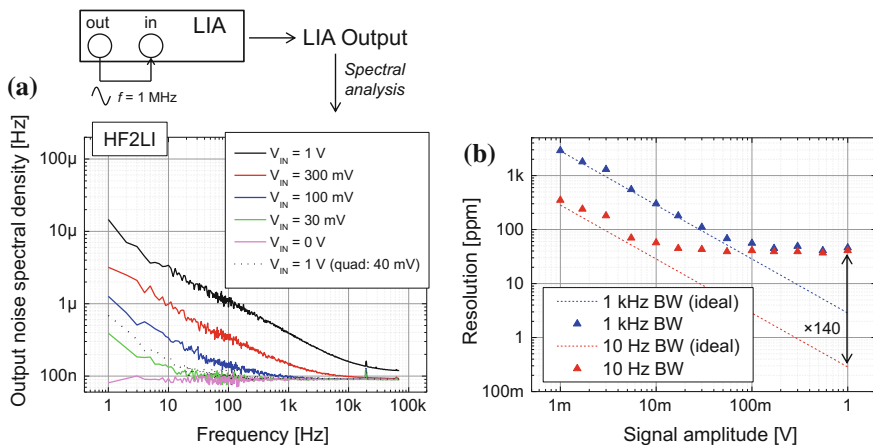


**Fig. 4** **a** Noise spectral densities of the demodulated LIA output obtained directly connecting the output terminal to the input of the commercial HF2LI. In addition to the white noise, a  $1/f$  contribution proportional to the signal amplitude is present. The dashed line refers to the noise in the quadrature output with a DC value of 40 mV, **b** resolution obtained with the HF2LI (directly connecting output and input of the instrument and performing measurements 100 s long) for different signal amplitudes and two filtering bandwidths (1 kHz and 10 Hz)

This limitation is confirmed by Fig. 4b, which shows the resolution obtained using the same setup of Fig. 4a and varying the signal amplitude (from 0 to 1 V) and filtering bandwidth (10 Hz and 1 kHz). For comparison, the figure also reports the expected theoretical result considering only the instrument white noise measured for  $V_{OUT} = 0$  V. By increasing the signal amplitude, the resolution reaches a plateau of about 40 ppm independently of the measurement bandwidth fixed by the low-pass filter. The resolution degradation due to the additional  $1/f$  noise results remarkable. For example, with a 1 V signal amplitude and 10 Hz low-pass filter, it would be ideally achievable a noise of  $280 \text{ nV}_{rms}$  and a corresponding resolution of about 0.28 ppm instead of the measured 40 ppm, a factor 140 worse.

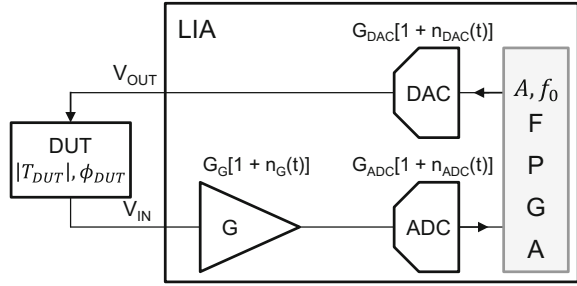
### 3.2 Flicker Noise Sources Identification

Benchtop digital LIAs commonly implement a homodyne detection in the digital domain in order to overcome the limitations of analog multipliers in terms of dynamic range, voltage offset and output noise. In particular, a digital demodulator is ideally free from  $1/f$  noise and by operating the digital LIA at frequencies where the noise of the analog circuitry is white, also the noise level at the output of the instrument should be white.

Since the additional  $1/f$  noise is proportional to the signal amplitude, the role of the waveform generator of the LIA has been investigated. The noise added to the



**Fig. 5** Visualization of the various multiplicative blocks along the signal path in a digital LIA, affected by slow gain fluctuations which set the resolution limit as detailed in (Eq. 5)



sinusoidal waveform by the output stage of the generator is modulated by the digital demodulator of the LIA giving a non-flicker noise at the output of the instrument, thus cannot explain the obtained results. The phase noise of the signal generator has been discarded as well. In fact, although its contribution is proportional to the signal, it would produce a noise level of the quadrature term higher than the noise of the in-phase term ([1], pp. 71–73). On the contrary, experimental evidence (Fig. 4a) shows a noise of the quadrature term much smaller than the in-phase noise.

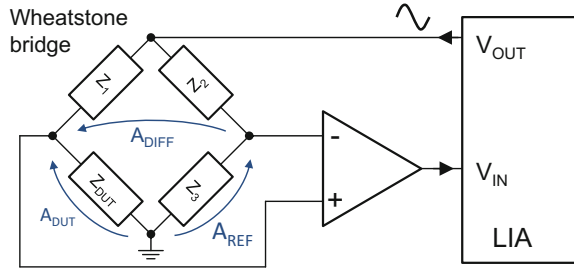
A further noise term of a waveform generator is the amplitude noise. A random modulation of the amplitude of the sinusoidal signal is down-converted by the LIA giving an additional noise in the in-phase component (or in the signal amplitude modulus), in agreement with the experimental results. Indeed, every component defining the amplitude of the signal, not only in the generation but also in the acquisition chain, is a source of a random amplitude modulation if its gain fluctuates.

For example, the unavoidable  $1/f$  noise of the reference voltage used by the DAC and ADC results in signal amplitude modulation. In fact, if the DAC reference voltage increases, the corresponding output voltage range results stretched and signal amplitude increases, while if the ADC reference voltage increases, the digital signal processed by the LIA decreases. Similar effects can be originated from internal circuits of the ADC and DAC that define the conversion gains. Regarding the analog stages, the resistors setting the gain of the transfer function are examples of amplitude modulation sources. The intrinsic  $1/f$  noise and temperature fluctuations change the value of resistors and therefore the gain experienced by the signal. Figure 5 shows the effect of these gain fluctuations in a simplified LIA scheme, where the  $n_{DAC}$ ,  $n_{ADC}$  and  $n_G$  terms summarize the converters and analog stages different contributions to the fluctuations. The digital processor operates on the digital signal  $V_{dig}$  given by

$$V_{dig}(k) = A|T_{DUT}|(1 + n_{DAC})(1 + n_G)(1 + n_{ADC}) \cos(2\pi f_0 kT + \phi_{DUT}) \quad (5)$$

where  $A$  is the amplitude of the stimulus voltage and  $|T_{DUT}|$ ,  $\phi_{DUT}$  are the magnitude and phase at  $f_0$  of the DUT transfer function and  $T$  is the sampling period. The amplitude  $R$  measured by the LIA is

**Fig. 6** Example of a differential setup (bridge) for high-resolution measurements



$$R = 2\sqrt{X^2 + Y^2} = A|T_{DUT}|(1 + n_{DAC})(1 + n_G)(1 + n_{ADC}) \tag{6}$$

Thus, the slow gain fluctuations are reflected in slow fluctuations of the amplitude provided by the LIA, setting the resolution limit of the instrument independently of  $f_0$ . Whatever signal is measured, it will always be affected by the LIA gain fluctuations, so if these fluctuations are in the order of tens of ppm, it will not be possible to measure the signal with a better resolution.

### 4 Differential Measurements

The slow gain fluctuations of the LIA add a noise proportional to the signal. This gives a severe limitation of the minimum detectable variation of a relatively large signal. In order to improve the sensitivity in the measurement of a signal variation, one possible approach is to remove the large component of the signal that does not change in the time. This can be performed with differential configuration [13] between the signal to be measured and a reference signal.

An example of a differential scheme for the measurement of an impedance  $Z_{DUT}$  is the well-known Wheatstone bridge reported in Fig. 6. The LIA measures the difference  $A_{DIFF}$  between the DUT signal and a reference signal. If the bridge is balanced, it gives a null signal  $A_{DIFF}$ , making negligible the amplitude-dependent noise produced by the input of the digital LIA. The reference signal is generated starting from the same wave generator applied to the DUT arm, thus its noise is cancelled out by the differential approach as well. The more the reference signal is similar (at any given time) to the DUT signal, the smaller is the differential signal and the less is demanded to the LIA in terms of resolution performance. This widely used technique allows measurements with resolution lower than 1 ppm, as reported for capacitance bridges [16, 17].

The differential solution can also be implemented for current measurements. In Fig. 7 are shown three differential schemes with a TransImpedance Amplifier (TIA) as current sensitive circuit. The difference can be achieved in current mode (i.e. at the virtual ground of the TIA before amplification) or in voltage mode (i.e. by means of a differential INA amplifier connected to the output of the TIA).

Current subtraction can be implemented in two ways. In Fig. 7a the sensor  $C_1$  is coupled with an identical replica  $C_2$ , with the common terminal connected to the virtual ground and the other terminal driven by an inverting buffer in counter-phase with  $V_{OUT}$ . If the two impedances are perfectly matched and the inverting buffer is ideal, all the current flowing in  $C_1$  flows in  $C_2$  and no current is amplified by the TIA, leading to a zero voltage at  $V_{IN}$ . Any unbalance between the two arms of the sensor (behaving as a half bridge with differential driving) produces a nonzero current signal that is amplified and demodulated by the LIA. When the technology does not allow the fabrication of a differential sensor, a separate compensation impedance (such as the dummy capacitor  $C_C$  in Fig. 7b) could be added of a value close to the expected sensor impedance ( $C_S$  in Fig. 7). In this solution, a variable-gain inverting amplifier (G) allows precise tuning of the counter-injected current to obtain perfect cancellation, i.e. accurate matching between the currents in  $C_C$  and in  $C_S$ . Similarly, solution in Fig. 7c consists in the addition of a full signal chain in parallel to the sensor impedance  $Z_S$ , including a dummy impedance  $Z_C$ , a second TIA and, if necessary, a phase shifter to be tuned, together with  $R_{FC}$ , to adjust the magnitude and phase of this auxiliary signal path. The output voltage of the dummy path is subtracted to the signal path by a differential amplifier, leading to only the residual small signal to be processed by the LIA.

The details of the hardware implementation of solutions (a) and (c) are reported in specific works, focusing on capacitive sensing of dust microparticles in air [10] and on detection of magnetic beads guided by nano-magnetic rails in liquid [18] respectively.

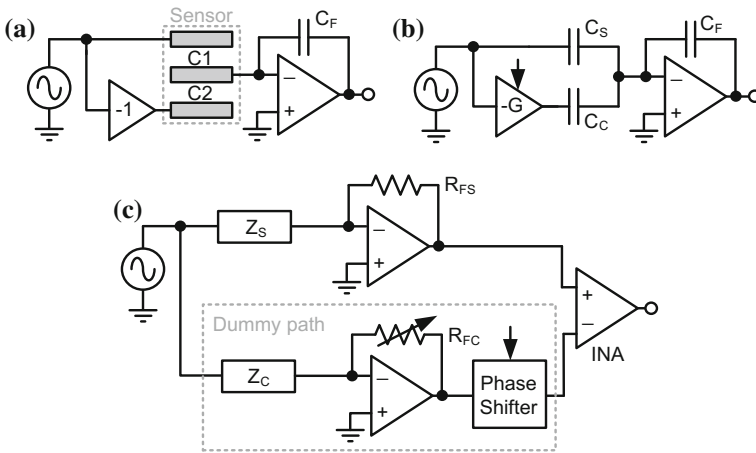


**Fig. 7** Differential configurations with a subtraction in current mode: **a** for matched sensors  $C_1 - C_2$  and **b** with tunable gain  $G$  to match  $C_C$  with  $C_S$ . **c** Differential subtraction in voltage mode of a compensation signal coming from a parallel dummy path with tunable gain ( $R_{FC}$ ) and phase (reprinted with permission from [13])

Here the experimental results obtained with these two implementations and using the HF2LI are reported. For solution (a), employing a TIA with capacitive feedback ( $C_F = 1$  pF) and a triplet of matched band electrodes, the switch from a single couple of electrodes to a differential configuration allows a reduction of the noise from 30 aF down to 1.1 aF ( $V_{OUT} = 1$  V,  $f_{AC} = 1$  MHz,  $BW = 1$  Hz). The resolution is improved by a factor of 27 reaching  $\approx 2$  ppm. The performance is still limited by the slow fluctuations of the lock-in amplifier because of the imperfect matching of C1 and C2 (mismatch of 5% limited by lithography of the microelectrodes). For solution (c), the activation of the dummy impedance path and the subtraction at the lock-in input ( $V_{OUT} = 50$  mV due to the liquid environment [18],  $f_{AC} = 2$  MHz,  $BW = 1$  Hz) reduces the conductance noise from 28 nS down to 2.6 nS. In both examples, the reduction of the signal at the input of the lock-in amplifier given by the differential approach has allowed an improvement of the resolution better than an order of magnitude.

Although the differential approach obtains excellent results, the generation of a well-balanced reference signal starting from the same signal source applied to the DUT could be cumbersome. The amplitude and phase of the reference signal has to match the DUT signal for every bias condition, operating temperature and frequency of measurement. Consequently, a calibration process is generally required for every DUT and measurement condition, adding complexity to the system and to the measurement itself.

## 5 Switched Ratiometric LIA Architectures

In order to enhance the LIA resolution performance, without the restrictions imposed by the differential approach, its gain fluctuations should be reduced. Regarding the analog conditioning stages, this can be obtained by implementing resistors with a low temperature coefficient ( $< 5$  ppm/K) where necessary, i.e. where resistors set the signal transfer function of the instrument [14]. Such components are less sensitive to temperature variations and are usually associated with a low intrinsic  $1/f$  noise (thus with lower resistance value variations). Instead, regarding the DAC and ADC, which are the major fluctuations contributors in our custom LIAs, there are no studies suggesting a way to reduce the effects of both of them. The simple solution of a common voltage reference would allow the cancellation of the reference effect, but it is not effective for the internal fluctuation sources of ADC and DAC converters such as, for instance, the  $1/f$  noise of a simple buffer at the reference input.

### 5.1 Digital Switched Ratiometric LIA with a Single ADC

The effect of gain fluctuations added by the DAC and all the generation chain can be reduced using the ratiometric technique, a well-known approach. For example it

is a common solution to compensate the light source intensity fluctuations in optical measurements [19]. In LIAs, the acquisition of the stimulus (STIM) signal in addition to the DUT signal (Fig. 8a) and their separate processing with a standard lock-in approach, produces two measured amplitudes ( $A_{DUT}$  and  $A_{STIM}$ ), both proportional to the gain fluctuations of the DAC (and generation chain). Thus, a ratio operation between the two amplitudes gives a value independent of the fluctuations of the generation stage (in Fig. 8 the effect of the analog stages is not considered). The phase can be retrieved as a simple difference between the DUT phase and the STIM phase. Since the phase is less sensitive to a random amplitude modulation, in the following we only analyze the measurement of the amplitude.

This first approach is not effective in many cases because of the gain fluctuations of the two independent ADCs, which are not compensated. In order to also remove their effect, a novel switched ratiometric approach has been conceived. A first single-ADC version, relies on the acquisition of both DUT and the STIM signals with the same ADC, which allows them to be equally affected by the ADC gain fluctuations and consequently to cancel out their effect through a ratio operation. Figure 8b shows the architecture of this switched ratiometric LIA with single ADC. A switch SW periodically changes the input of the ADC alternating the DUT and the STIM signals. The switching frequency is chosen fast enough to assume the same ADC gain for the DUT samples and the STIM samples in a switching period. The digital processor separates the digitized samples in order to reconstruct the two signals in the digital domain, implements the synchronous demodulation of them and finally calculates the ratio of the amplitudes. Although the gain fluctuations are slow (up to few kHz from Fig. 4a), the switching frequency of SW should be chosen fast enough to satisfy the sampling theorem in order to avoid loss of information. Such a condition is difficult to be fulfilled in the case of high frequency digital LIAs, with sampling rate of tens or hundreds of MS/s, in particular for the voltage transients given by the switching of the ADC input.

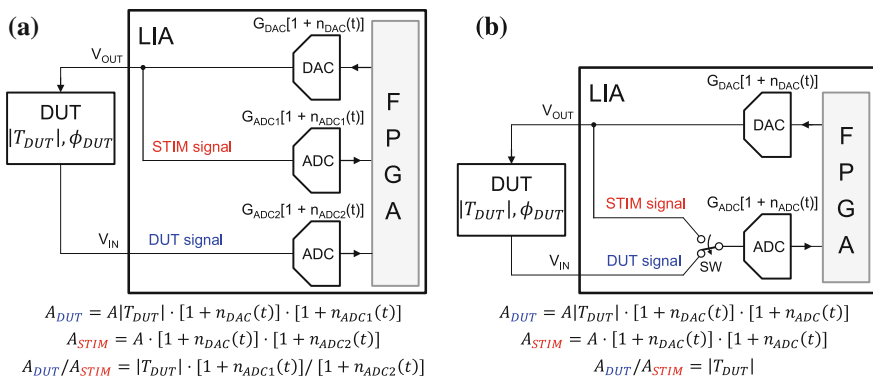


**Fig. 8** **a** Simplified scheme implementing a ratiometric measurement. **b** Simplified scheme of a switched ratiometric LIA based on a single ADC

### 5.2 Digital Switched Ratiometric LIA Based on Two ADCs

In order to reduce the switching frequency required by the scheme of Fig. 8b, an architecture based on two ADCs, as shown in Fig. 9, has been recently proposed and is patent pending. Two switches SW1 and SW2 are added in front of the ADCs to alternatively acquire the DUT and the STIM signals with each ADC. The signals are reconstructed in real-time using a FPGA to obtain their time evolution with continuity in the digital domain. The following demodulation and averaging are performed as in a standard dual-phase LIA obtaining amplitude and phase of the DUT and STIM signals. The switching frequency  $f_{SW}$  of SW1 and SW2 is chosen of few kHz, that is faster than the slow random gain fluctuations of the ADCs. As a consequence, the equivalent gain in a period  $1/f_{SW}$  experienced by the two reconstructed signals is the same and is equal to the mean of the two ADC gains. The effect of the gain fluctuations is finally canceled out by performing the ratio between the amplitudes of the DUT and STIM signals. Obviously, the gain fluctuations of the DAC are also included in both signals and therefore removed as well, allowing a high-resolution measurement of the DUT signal.

### 5.3 Theoretical Analysis

Here the working principle of the presented switched ratiometric scheme is mathematically analyzed. Then, some considerations on the harmonics generated by the switching operation and how to prevent them from causing performance degradation are made.

The two digitally reconstructed signals DUT and STIM (Fig. 9) can be represented by:

$$S_{DUT}(t) = A|T_{DUT}| \cos(2\pi f_0 t + \varphi_{DUT}) \cdot [G_{ADC1}(t)\phi_{SW}(t) + G_{ADC2}(t)(1 - \phi_{SW}(t))] \quad (7)$$

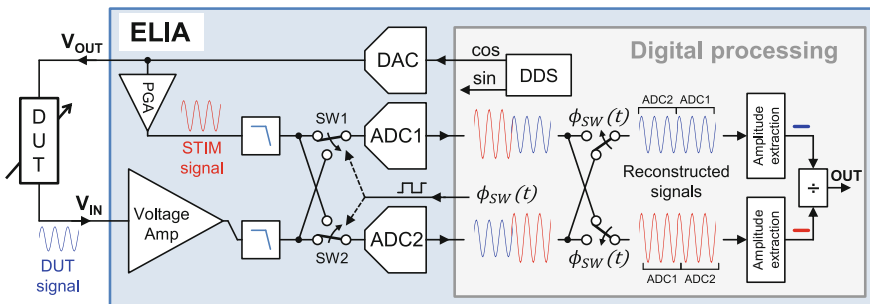
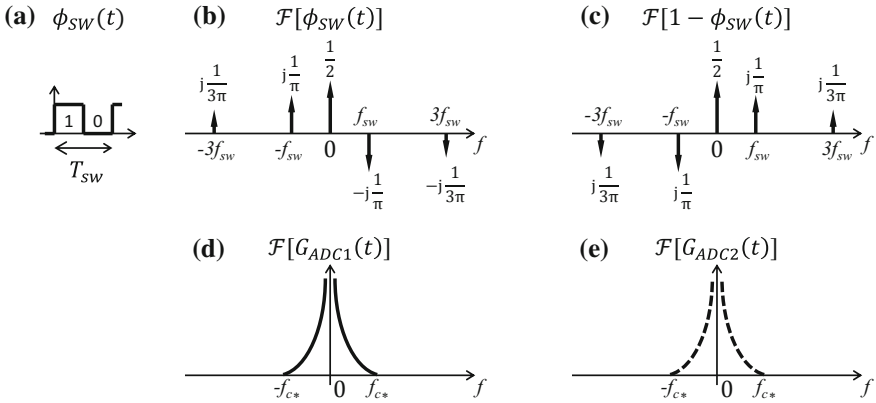


Fig. 9 Architecture of a switched ratiometric LIA based on two ADCs



**Fig. 10** Fourier transforms of the square wave signals  $\phi_{SW}$  (b) and  $1 - \phi_{SW}$  (c) and of the ADCs gains  $G_{ADC1}(t)$  (d) and  $G_{ADC2}(t)$  (e)

$$S_{STIM}(t) = A \cos(2\pi f_0 t) \cdot [G_{ADC2}(t)\phi_{SW}(t) + G_{ADC1}(t)(1 - \phi_{SW}(t))] \quad (8)$$

where  $\phi_{SW}(t)$  is a square wave (0–1) with a duty cycle of 50% and period  $T_{SW}$  (as shown in Fig. 10a).  $|T_{DUT}|$  is the magnitude at  $f_0$  of the DUT transfer function. For simplicity is assumed  $\varphi_{DUT} = 0$  and neglected the noises of DAC, analog stages and quantization.

These reconstructed signals are demodulated in phase and quadrature by the lock-in amplifier. The in-phase component (multiplication by  $\cos(2\pi f_0 t)$ ) is:

$$S_{DUT,demod}(t) = \frac{A}{2} |T_{DUT}| [G_{ADC1}(t)\phi_{SW}(t) + G_{ADC2}(t)(1 - \phi_{SW}(t))] + \frac{A}{2} |T_{DUT}| [G_{ADC1}(t)\phi_{SW}(t) + G_{ADC2}(t)(1 - \phi_{SW}(t))] \cos(2\pi 2f_0 t) \quad (9)$$

$$S_{STIM,demod}(t) = \frac{A}{2} [G_{ADC2}(t)\phi_{SW}(t) + G_{ADC1}(t)(1 - \phi_{SW}(t))] + \frac{A}{2} [G_{ADC2}(t)\phi_{SW}(t) + G_{ADC1}(t)(1 - \phi_{SW}(t))] \cos(2\pi 2f_0 t) \quad (10)$$

These two signals can be studied performing the Fourier transform and exploiting the convolution theorem. Although Eqs. 9 and 10 are characterized by two terms, it is useful to start taking into account only the first one, while the second one, multiplied by  $\cos(2\pi 2f_0 t)$ , will be treated successively:

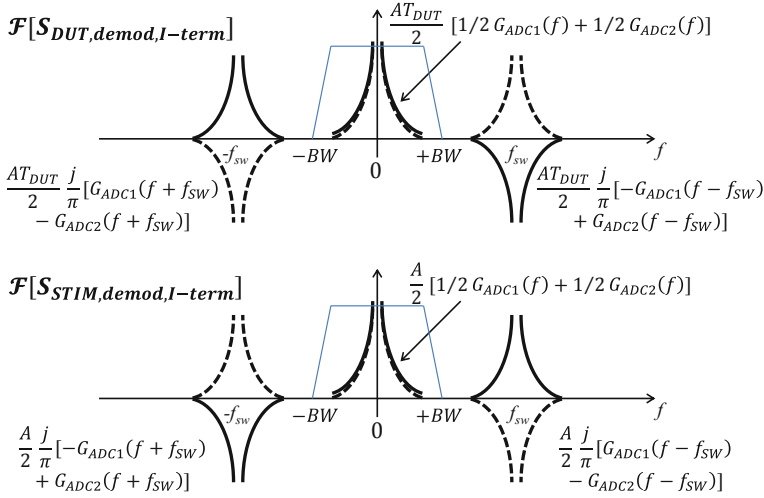


**Fig. 11** Spectra obtained from the sum and convolution of the various terms of Eqs. 11 and 12. For graphical clarity the successive harmonics at  $\pm 3f_{sw}$ ,  $\pm 5f_{sw}$ , etc. are not depicted

$$\mathcal{F}\{S_{DUT,demod,I-term}(t)\} = \frac{A}{2} |T_{DUT}| \cdot \{\mathcal{F}[G_{ADC1}(t)] * \mathcal{F}[\phi_{sw}(t)] + \mathcal{F}[G_{ADC2}(t)] * \mathcal{F}[1 - \phi_{sw}(t)]\} \quad (11)$$

$$\mathcal{F}\{S_{STIM,demod,I-term}(t)\} = \frac{A}{2} \cdot \{\mathcal{F}[G_{ADC2}(t)] * \mathcal{F}[\phi_{sw}(t)] + \mathcal{F}[G_{ADC1}(t)] * \mathcal{F}[1 - \phi_{sw}(t)]\} \quad (12)$$

In order to compute the Fourier transform of the two signals (Eqs. 11 and 12) it is useful to compute and represent the Fourier transform of their various terms. The Fourier transform of the square wave signals  $\phi_{sw}$  and  $1 - \phi_{sw}$  are described by a series of Dirac delta functions at frequency  $0, \pm f_{sw}, \pm 3f_{sw}$ , etc. (as represented in Figs. 10b, c)<sup>3</sup>. The Fourier transforms of  $G_{ADC1}(t)$  and  $G_{ADC2}(t)$  are sketched in Figs. 10d, e and are characterized by a  $1/f$  noise<sup>4</sup> which becomes negligible starting from a frequency defined  $f_{c*}$ , while their white noise is neglected.

In Fig. 11 the spectra obtained from the sum and convolution of the various terms are shown. In DC, both the signals of interest  $\frac{AT_{DUT}}{2}$  and  $\frac{A}{2}$  from the demodulated sig-

<sup>3</sup>Rigorously the Fourier transform should be represented by the real and imaginary part or by module and phase. For simplicity real and imaginary parts are here combined in a single graph.

<sup>4</sup>In Fig. 10 the Fourier transforms of  $G_{ADC1}$  and  $G_{ADC2}$  are qualitatively sketched with their spectral power density. The analysis in the main text uses the Fourier transform which has the important feature of keeping the phase information, unlike the power spectral density.



nals DUT and STIM respectively, are multiplied by the same factor  $\frac{G_{ADC1}(f)+G_{ADC2}(f)}{2}$ . This confirms the intuitive idea that the two signals (DUT and STIM) experience an equivalent gain given by the mean of the two ADCs gain. Instead, the terms at  $\pm f_{SW}$  and successive harmonics result multiplied by a different factor in DUT and STIM, which in both cases depends on the difference between the two ADC gains.

Finally, the LIA implements a low-pass filter of bandwidth  $BW$ . It is evident that it should cut the harmonics at  $\pm f_{SW}$  and successive, comprised their tails. The higher harmonics  $\pm 3f_{SW}$ ,  $\pm 5f_{SW}$ , etc. are not taken into account and represented in Fig. 11 because they are easier to be filtered and smaller respect to the first one. To study the effect of the successive ratio operation, it is useful to work in the time domain, thus the Fourier anti-transform is performed, obtaining:

$$S_{DUT,demod,I-term}(t) = \frac{A}{2} |T_{DUT}| \cdot \left\{ \frac{1}{2} [G_{ADC1}(t) + G_{ADC2}(t)] + \frac{1}{\pi} [G_{ADC1}(t) - G_{ADC2}(t)] \sin(2\pi f_{SW}t) \right\} \quad (13)$$

$$S_{STIM,demod,I-term}(t) = \frac{A}{2} \cdot \left\{ \frac{1}{2} [G_{ADC1}(t) + G_{ADC2}(t)] + \frac{1}{\pi} [G_{ADC2}(t) - G_{ADC1}(t)] \sin(2\pi f_{SW}t) \right\} \quad (14)$$

Looking at the terms between brackets we can notice that the first term of both Eqs. 13 and 14 is identical, while the second is not, as expected from the different spectra. Thus, in order to make the ratio operation effective in canceling the effect of  $G_{ADC1}(t)$  and  $G_{ADC2}(t)$ , it is important to filter the harmonics at  $\pm f_{SW}$  including their tails. From a different point of view, given a certain filtering bandwidth  $BW$  it is important to select  $f_{SW}$  in order to make the harmonics (and tails) stay out of the filtering bandwidth  $BW$ . Mathematically this necessary condition is:

$$f_{SW} > f_{c*} + BW \quad (15)$$

If this condition is satisfied, it is possible to write:

$$S_{DUT,demod,I-term}^{LPF}(t) = \frac{A}{2} |T_{DUT}| \left[ \frac{G_{ADC1}^{LPF}(t) + G_{ADC2}^{LPF}(t)}{2} \right] \quad (16)$$

$$S_{STIM,demod,I-term}^{LPF}(t) = \frac{A}{2} \left[ \frac{G_{ADC1}^{LPF}(t) + G_{ADC2}^{LPF}(t)}{2} \right] \quad (17)$$

and performing the ratio between the two signals:

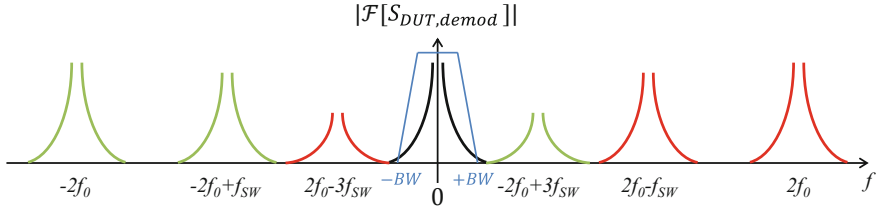


**Fig. 12** Useful demodulated DUT signal in DC and harmonics due to the second term (multiplied by  $\cos(2\pi f_0 t)$ ) of Eq. 9 which can fall into the measurement bandwidth  $\pm BW$ . The same spectral distribution is expected for the demodulated stimulus signal  $S_{STIM,demod}$

$$\frac{S_{DUT,demod,1-term}^{LPF}(t)}{S_{STIM,demod,1-term}^{LPF}(t)} = |T_{DUT}| \quad (18)$$

obtaining a measurement of the DUT independent of the two ADCs gain fluctuations.

If the second term of Eqs. 9 and 10 is taken into account, others harmonics appear, in particular at the frequencies  $2f_0$ ,  $2f_0 \pm f_{SW}$ ,  $2f_0 \pm 3f_{SW}$ , ...,  $-2f_0$ ,  $-2f_0 \pm f_{SW}$ ,  $-2f_0 \pm 3f_{SW}$ , ..., as shown<sup>5</sup> in Fig. 12. Also in this case it is important that the various harmonics with their tails do not fall into the bandwidth of interest between  $\pm BW$ . Looking at the bilateral spectrum of Fig. 12, in order to avoid harmonics in bandwidth  $\pm BW$  it is necessary to satisfy this condition<sup>6</sup>:

$$BW < 2f_0 - (1 + 2k)f_{SW} - f_{c*} \quad (19)$$

or this other condition:

$$2f_0 - (1 + 2k)f_{SW} + f_{c*} < -BW \quad (20)$$

for each natural number  $k$ . At this point it is possible to summarize the conditions in this way:

$$\begin{cases} f_{SW} > f_{c*} + BW \\ \{(1 + 2k)f_{SW} > 2f_0 + f_{c*} + BW \vee (1 + 2k)f_{SW} < 2f_0 - f_{c*} - BW\} \end{cases} \quad (21)$$

In some practical cases, these conditions are considerably simplified. In particular if a narrow bandwidth  $\pm BW$  is assumed (much smaller than  $f_{c*}$ ) and if the switching frequency  $f_{SW}$  is much higher than  $f_{c*}$ , the conditions becomes:

<sup>5</sup>Only the modulus of the Fourier transform is represented.

<sup>6</sup>The conditions are easily written by considering the components produced by the  $2f_0$  term (red harmonics in Fig. 12). The harmonics from  $-2f_0$  (in green) are specular and give the same conditions.

$$\begin{cases} BW \ll f_{c*} \\ f_{SW} \gg f_{c*} \\ (1 + 2k)f_{SW} \neq 2f_0 \end{cases} \quad (22)$$

the last condition must be satisfied with a certain margin (at least the value of  $f_{c*}$ ) given the performed approximations.

Obviously, working with  $f_0 - BW < f_{SW} < f_0 + BW$  is also not a convenient condition. In particular, due to the risk of injecting into the ADCs inputs a feedthrough signal (given by the switches commutations) which exactly falls into the modulated signal bandwidth.

## 6 Enhanced-LIA Board Realization

An enhanced-LIA (ELIA) instrument based on the switched ratiometric technique has been realized and fully characterized. The prototype comprises a generation channel, two identical acquisition channels and is controlled by a Xilinx Spartan 6 FPGA mounted on a commercial module XEM 6010 by Opal Kelly connected to the board, which also provides an USB interface.

Figure 13 represents the hardware scheme of the realized board. The elements whose gain fluctuations are compensated by the switched ratiometric technique are highlighted in blue. The detailed board design is described here [20].

### 6.1 Analog Architecture Design Details

#### *Switches Position*

The switched ratiometric technique allows compensating the gain fluctuations of the stages following the switches. For this reason, it could be useful to insert the switches as the first stage of the acquisition channels. Nevertheless, in this first implementation, it was decided to implement them just before the ADCs for two reasons: (i) the dominating gain fluctuations source is the ADC; (ii) the samples immediately after the switching of SW1 and SW2 are correctly acquired thanks to the fast differential OpAmp and switches. Figure 14 shows the experimental acquisition and reconstruction of the DUT and STIM signals during the swap between the two ADCs operated by SW1 and SW2. A fast recovery of the correct signals value, after about three acquisition samples (37.5 ns), is shown. With the switches as first stage, the last condition would not be satisfied due to the settling time of the anti-aliasing filter. The noise folding due to the fast differential OpAmp has been taken into account, and its noise results negligible at the end of the acquisition chain.

#### *Not Compensated Gain Fluctuations*

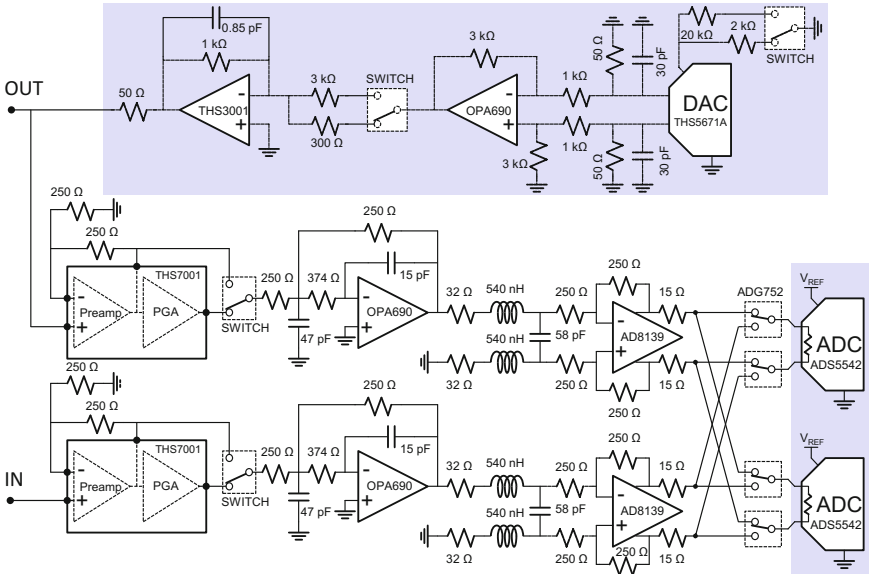
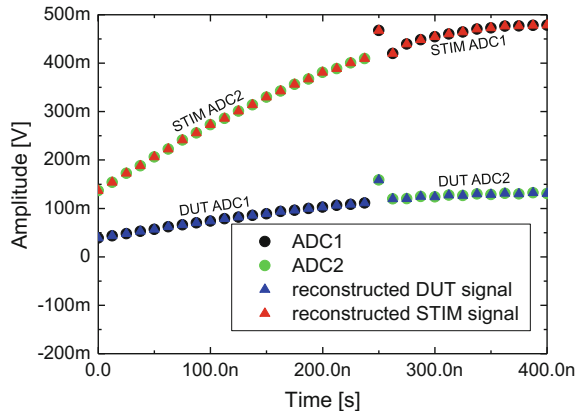


**Fig. 13** Detailed hardware scheme of the ELIA instrument. The gain fluctuations of the components in the *shaded boxes* are compensated by the switched ratiometric technique

**Fig. 14** Acquisition and reconstruction of the DUT and STIM signals during the swap between the two ADCs. The values are referred to the input of the ADCs, which have a dynamic of  $\pm 1.1$  V. In this case, after a step of about 300 mV, thanks to the fast settling time of the AD8139, the reconstructed signals reach the correct value (error  $< 1\%$ , i.e.  $< 4$  mV) after about three samples (37.5 ns)



The gain fluctuations of the elements located in the two independent acquisition paths, from the pre-amplifier to the switches, are not compensated by the switched ratiometric technique. In particular, the elements to be considered are: (i) the resistors involved in the channel transfer function; (ii) the PGAs; (iii) the switches before the ADCs.

In order to minimize the resistors effect, non-standard resistors characterized by low thermal coefficient ( $< 5$  ppm/K) and low  $1/f$  intrinsic noise, have been employed [14].

Temperature fluctuations also vary the PGAs gain, characterized by a gain temperature coefficient of about 25–35 ppm/K [21]. Experimental results show a small performance degradation when the two PGAs are not by-passed (from 0.6 to 0.85 ppm as shown in the next section). However, it is important to notice that integrated circuits comprising two PGAs with a good channel-to-channel gain temperature coefficient match (few ppm/K) are available [22]. This feature will be considered for future implementations.

Regarding the switches network, it is important to consider the voltage divider between the switch resistance and the finite differential input resistance of the ADS5542 ADCs, specified of  $R_{ADC} \approx 6.6 \text{ k}\Omega$ . A random fluctuation of the ADC input resistance is not an issue itself, because its effect is compensated by the technique. Instead, the resistance of the switches can vary independently each other, causing uncorrelated fluctuations of the two signals acquired by the ADCs. To reduce their effect, low resistance ( $R = 15 \text{ }\Omega$ ) switches have been selected. This way, their fluctuations affect the transfer function by a reduced factor  $R_{SW}/(R_{SW} + 15\Omega + R_{ADC}) \approx 0.0023$ .

## 6.2 Digital Architecture Additional Modules

Only two additional digital modules, with respect to a standard LIA, are required as shown in Fig. 15. The first is a module to reconstruct in the digital domain the DUT and STIM signals by taking alternatively the samples from the two ADCs coherently with the position of the switches. A delay block allows to set the correct timing for the signals reconstruction considering the acquisition pipeline delay. The second module simply calculates the amplitudes of the DUT and STIM signals and operates the division between them to remove the gain fluctuations.

## 7 Results

In this chapter the effectiveness of the switched ratiometric technique and the correctness of the previous theoretical analysis are demonstrated. In particular, it is shown that this technique enhances the ELIA instrument resolution limit by more than an order of magnitude (from 9 to 0.6 ppm). After a first technique assessment with a simple resistive DUT, the ELIA instrument has been used to measure a more complex DUT, demonstrating its performance independence from changes in the DUT signal phase and amplitude. Another experiment confirmed the importance of selecting a switching frequency greater than the  $1/f$  noise corner frequency of the single channel as expected.

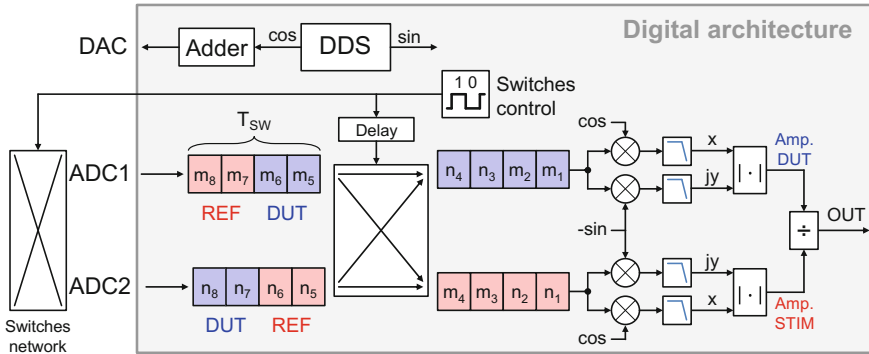


**Fig. 15** DUT and STIM signals acquisition and processing chain: after analog-to-digital conversion, the signals are coherently reconstructed taking in consideration the delay between the analog switches and the converted digital words. Successively are processed as in standards LIAs and finally the ratio between the two obtained amplitudes is performed

## 7.1 Assessment of the Resolution Capability of ELIA

In order to verify the effectiveness of the switched ratiometric technique, a sinusoidal signal of 1 V at a frequency of 1 MHz has been generated and applied to the input of ELIA through a resistive voltage divider as shown in Fig. 16a. In the first experiment, whose results are reported in Fig. 16b, the DUT and STIM signals have been separately acquired with a specific ADC. The demodulated signals are normalized and the fluctuations appear of the same amplitude (about 9 ppm), but not correlated. Although the DAC fluctuations are shared by the two signals, the ones of the two ADCs are indeed uncorrelated, making this simple ratiometric approach ineffective. In a second experiment, the switches have been enabled to perform the switched ratiometric technique. In this case the fluctuations of the reconstructed DUT and STIM signals are clearly correlated (Fig. 16c). Thus, they can be effectively reduced by means of a ratio operation, obtaining a residual uncertainty of only 0.7 ppm in this case (Fig. 16d). Given the obtained results and the fact that the DUT and STIM signals are of different amplitude (0.5 and 1 V respectively), the demodulated output fluctuations cannot be related to an additive noise, but necessarily to gain fluctuations.

As second experiment to evaluate the ELIA performance, Fig. 17a shows the tracking of a time-varying resistance of 250  $\Omega$  periodically changed (period of 10 s) of  $\Delta R = 1.25$  m $\Omega$ , i.e. 5 ppm. The measurement has been performed in three different conditions: (i) using the commercial HF2LI by Zurich Instruments; (ii) using ELIA as a standard lock-in amplifier (i.e. only measuring the DUT signal with a single acquisition channel); (iii) using ELIA with the switched ratiometric technique here proposed (with  $f_{SW}$  set to 1 kHz). The signal amplitude applied to the time-varying resistance is 300 mV, the signal frequency is of 3.2 kHz and the filtering bandwidth of 1 Hz. The resolution enhancement of more than an order of magnitude, from 9 ppm to 0.6 ppm, given by the switched ratiometric technique, allows a clear

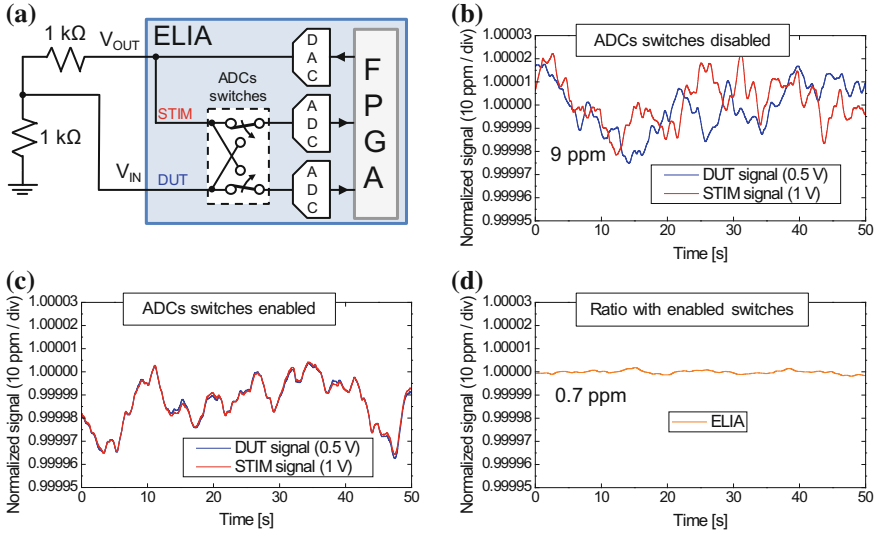


**Fig. 16** Demonstration of the technique effectiveness in making the DUT and STIM signals experience the same gain fluctuations in order to allow their cancellation by means of a simple ratio

detection of the tiny (5 ppm) resistance modulation, which is completely masked by noise in standard LIA implementations, as reported in Fig. 17a. Figure 17b shows the measured noise spectra at the LIAs output in the same three experimental conditions. In order to obtain noise spectra going up to 1 kHz, the LIAs frequency has been increased at 100 kHz, the filtering BW at 1 kHz, selected an internal switches frequency  $f_{sw} = 2$  kHz and the modulation of the DUT resistance has been disabled. The spectra clarify that the performance improvement given by the switched ratiometric technique is due to a substantial reduction of the  $1/f$  noise affecting the standard implementations. The technique improves the resolution not only with narrow low-pass filtering ( $BW \leq 1$  Hz), but also with higher filtering bandwidths.

### 7.2 Independence from Signal Phase and Amplitude

Differently from a differential technique, the effectiveness of the switched ratiometric technique is in principle insensitive to the phase and amplitude relationship between the DUT and STIM signals. In order to experimentally prove it, the instrument has been tested with an R-RC network. Figure 18a, b shows the measured transfer function, characterized by a change of a factor 5 of the amplitude and of about  $\angle(\pi/4)$  of the phase. In Fig. 18c is shown the measurement resolution at every specific frequency. Sub-ppm performance ( $< 1$  ppm) have been achieved up to about 5 MHz, demonstrating an operation insensitive to the signal phase and amplitude.

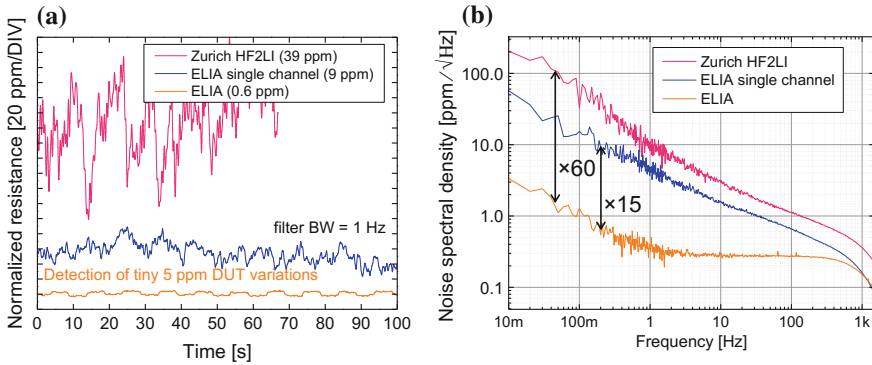


**Fig. 17** Comparison of performance between standard LIA implementations and the switched ratiometric ELIA instruments. Thanks to the better performance of the latter tiny DUT variations of 5 ppm are measurable. The improvement is apparent both in frequency (a) and time domain (b)

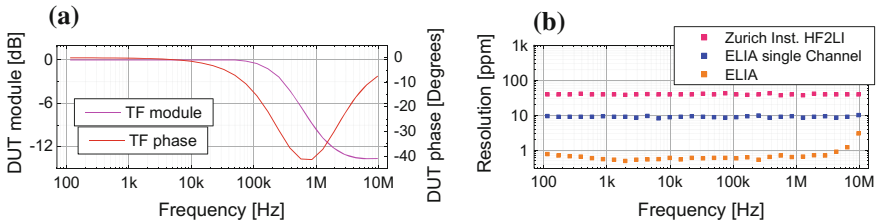


**Fig. 18** Measured transfer function TF of the test complex network a used to assess the effect of amplitude and phase changes of the DUT signal. The resolution is *below* 1 ppm up to about 5 MHz independently of the DUT signal changes with respect to the STIM one (b)

The performance degradation observed for frequencies higher than 5 MHz can be explained by the channel transfer function. At 6 MHz it is decreased by 2% due to anti-aliasing filtering and is starting to rapidly decrease. It means that the capacitors value, characterized by a poor thermal coefficient of 30 ppm/K, becomes increasingly important in defining the transfer function, thus possibly decreasing the resolution performance (about 3 ppm at 10 MHz).

The insensitiveness of the ELIA instrument to the amplitude and phase of the DUT signal with respect to the STIM signal, allows it to operate as a standard LIA, which does not require calibration steps at any new experiment or measurement frequency change, as happen with a differential approach.

### 7.3 Resolution and Switching Frequency

Consistently with the discussion in Sect. 5.3, a relation between the switches frequency  $f_{SW}$  and the instrument resolution has been experimentally observed. Figure 19a shows the noise spectrum obtained with the ELIA instrument, but only



using a single channel (the DUT channel) as in standard implementations. The stimulus frequency has been set to 500 kHz and the instrument output directly connected to the input. The obtained  $1/f$  noise corner frequency  $f_c$  is about 1 kHz. Figure 19b shows the resolution obtained enabling the switched ratiometric technique and varying  $f_{SW}$ . The filtering bandwidth was 1 Hz and each measurement was 100 s long. With a switching frequency greater than 1 kHz the resolution flats on sub-ppm values. On the contrary, by lowering  $f_{SW}$  the resolution gets worse due to the overlapping with the side harmonics  $1/f$  noise as discussed in Sect. 5.3. The time domain interpretation is that a significant gain fluctuation occurs during the switching period, thus the ADC gain and its fluctuations are not equivalent for the two signals DUT and STIM.

### 8 Conclusions

The maximum measurement resolution achievable using lock-in amplifiers is limited by an unexpected  $1/f$  noise proportional to the signal to be measured. The measurement resolution cannot be improved narrowing the filtering bandwidth, because the noise is  $1/f$ , neither increasing the signal amplitude, because the noise is signal-proportional, posing a fundamental limit.

The source of this  $1/f$  noise (and of the resolution limit) has been identified in the effect of gain fluctuations of various elements of the generation and acquisition chain, in particular due to the digital-to-analog and analog-to-digital converters.

A differential approach reduces the effects of the gain fluctuations, enabling the measurement of small variations. However, it requires the design of a reference path matched to the signal path for all the experimental conditions. In order to simplify the experimental setup and avoid a calibration step of the reference, a LIA based on two

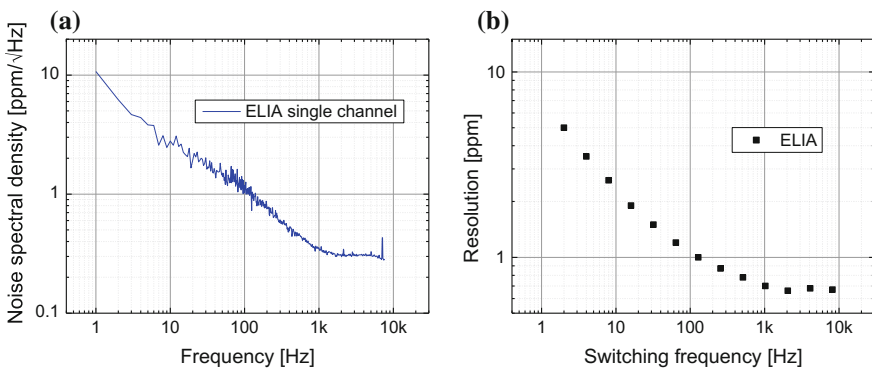


**Fig. 19** Resolution dependence on the switching frequency. To achieve the best performance the condition  $f_{SW} > f_c + BW$  (Eq. 15 of Sect. 5.3) needs to be satisfied, in this case equivalent to  $f_{SW} > 1kHz$

ADCs alternately acquiring the signal coming from the Device Under Test (DUT) and the stimulus (STIM) signal, has been conceived. This enhanced-LIA allows the compensation of the slow gain fluctuations of both DAC and ADC, considerably reducing their effect on the measurements.

Experimental results demonstrate the technique effectiveness. It allows enhancing the instrumentation resolution limit by a factor 15, from 9 to 0.6 ppm, a resolution value which is considerably better than the examined state-of-the-art LIA standard implementations working up to similar frequencies, as shown in Table 1.

The technique does not require additional external elements or accurate case-by-case calibrations, two typical constraints of the alternative differential technique. Instead, it only requires to satisfy some defined conditions when choosing the switching frequency of the internal ADCs switches.

**Acknowledgements** The authors would like to thank Prof. M. Sampietro for his stimulating interest in this work and for sharing laboratory resources, and Filippo Campoli for the help with the experimental measurements. Financial support by Fondazione Cariplo under Projects Minute and Drinkable and by the European Union under grant agreement no. 688172 (H2020-ICT-STREAMS project) are gratefully acknowledged.

## References

1. M.L. Meade, *Lock-in Amplifiers: Principles and Applications* (Peter Peregrinus Ltd., 1983)
2. G. Gervasoni, M. Carminati, G. Ferrari, A general purpose lock-in amplifier enabling sub-ppm resolution, in *Euroensors 2016, Proceedings* (2016)
3. P. Ciccarella, M. Carminati, M. Sampietro, G. Ferrari, Multichannel 65 zF rms resolution CMOS monolithic capacitive sensor for counting single micrometer-sized airborne particles on chip. *IEEE J. Solid-State Circ.* **51**(11), 2545–2553 (2016)
4. L. Fumagalli, G. Ferrari, M. Sampietro, G. Gomila, Quantitative nanoscale dielectric microscopy of single-layer supported biomembranes. *Nano Lett.* **9**(4), 1604–1608 (2009)
5. T. Tran, D.R. Oliver, D.J. Thomson, G.E. Bridges, Zeptofarad (10<sup>sup</sup> 21]F) resolution capacitance sensor for scanning capacitance microscopy. *Rev. Sci. Instrum.* **72**(6), 2618 (2001)
6. C.-S. Liao, M.N. Slipchenko, P. Wang, J. Li, S.-Y. Lee, R.A. Oglesbee, J.-X. Cheng, Microsecond scale vibrational spectroscopic imaging by multiplex stimulated Raman scattering microscopy, in *Light: Science & Applications*, August 2014, vol. 4 (2015), p. e265
7. V. Kumar, N. Coluccelli, M. Cassiniero, M. Celebrano, A. Nunn, M. Levrero, T. Scopigno, G. Cerullo, M. Marangoni, Low-noise, vibrational phase-sensitive chemical imaging by balanced detection RIKE. *J. Raman Spectrosc.* **46**(1), 109–116 (2014)
8. T. Sun, H. Morgan, Single-cell microfluidic impedance cytometry: a review. *Microfluid. Nanofluid.* **8**(4), 423–443 (2010)
9. N. Haandbæk, O. With, S.C. Bürgel, F. Heer, A. Hierlemann, Resonance-enhanced microfluidic impedance cytometer for detection of single bacteria, in *Lab on a Chip*, vol. 14, no. 17 (2014), pp. 3313–3324
10. M. Carminati, L. Pedalà, E. Bianchi, F. Nason, G. Dubini, L. Cortelezzi, G. Ferrari, M. Sampietro, Capacitive detection of micrometric airborne particulate matter for solid-state personal air quality monitors. *Sens. Actuators A Phys.* **219**, 80–87 (2014)
11. M. Carminati, G. Ferrari, M. Sampietro, Attofarad resolution potentiostat for electrochemical measurements on nanoscale biomolecular interfacial systems. *Rev. Sci. Instrum.* **80**, 12 (2009)
12. SRS, About lock-in amplifiers. *Appl. Note* **408**, 1–9 (2011)

13. M. Carminati, G. Gervasoni, M. Sampietro, G. Ferrari, Note: differential configurations for the mitigation of slow fluctuations limiting the resolution of digital lock-in amplifiers. *Rev. Sci. Instrum.* **87**, 2 (2016)
14. G. Gervasoni, M. Carminati, G. Ferrari, M. Sampietro, E. Albisetti, D. Petti, P. Sharma, R. Bertacco, A 12-channel dual-lock-in platform for magneto-resistive DNA detection with ppm resolution, in *IEEE 2014 Biomedical Circuits and Systems Conference, BioCAS 2014—Proceedings* (2014), pp. 316–319
15. M. Carminati, A. Rottigni, D. Alagna, G. Ferrari, M. Sampietro, Compact FPGA-based elaboration platform for wide-bandwidth electrochemical measurements, in *2012 IEEE I2MTC—International Instrumentation and Measurement Technology Conference, Proceedings*, no. 214706 (2012), pp. 264–267
16. M.C. Foote, A.C. Anderson, Capacitance bridge for low-temperature, high-resolution dielectric measurements. *Rev. Sci. Instrum.* **58**(1), 130 (1987)
17. ANDEEN-HAGERLING, *AH 2700A datasheet*
18. M. Carminati, G. Ferrari, S.U. Kwon, M. Sampietro, M. Monticelli, A. Torti, D. Petti, E. Albisetti, M. Cantoni, R. Bertacco, Towards the impedimetric tracking of single magnetically trailed microparticles, in *2014 11th International Multi-Conference on Systems, Signals Devices (SSD)* (2014), pp. 1–5
19. PerkinElmer, *Low Level Optical Detection using Lock-in Amplifier Techniques* (2000)
20. G. Gervasoni, Novel architecture of digital lock-in amplifier for extremely high resolution measurements. Ph.D. thesis, Politecnico di Milano, 2016
21. Texas Instruments, *THS7001 datasheet*
22. Linear Technologies, *LTC6911-2 datasheet*